



Cite this: DOI: 10.1039/c8nj05671d

Highly stable and bright fluorescent chlorinated polymer dots for cellular imaging†

 Daize Mo,^{ab} Zhe Chen,^c Liang Han,^b Hanjian Lai,^b Pengjie Chao,^b Qingwen Zhang,^{*a} Leilei Tian^{ib} ^{*c} and Feng He^{ib} ^{*b}

Chlorinated organic materials have drawn much attention and have been applied in various fields due to their intriguing properties such as easy accessibility with low cost, high capability to hold electron density, and “heavy-atom effect”. In this work, a kind of highly fluorescent chlorinated semiconducting polymer dot (PFDPICBT) is developed for cell imaging by using an amphiphilic polymer poly(styrene-co-maleic anhydride) as the co-encapsulation matrix. The PFDPICBT dots show a small particle size of about 50 nm, a large Stokes shift of 125 nm, quite high fluorescence quantum yields (QYs) of 20.3% (PFDPBT: 8.5%), and increased reactive oxygen species generation efficiency. Since the chlorinated Pdots are brighter than their non-chlorinated counterparts and can label the target cell effectively with low cytotoxicity, they are promising fluorescent probes in bioimaging applications.

Received 8th November 2018,
Accepted 8th January 2019

DOI: 10.1039/c8nj05671d

rsc.li/njc

Introduction

Conjugated polymers (CPs) have been widely applied in various fields of organic electronics/optoelectronics, such as organic field effect transistors (OFETs), organic light-emitting diodes (OLEDs), and organic photovoltaic cells (OPVs).¹ Owing to their excellent light-harvesting and light-amplifying properties, CPs could also be used as a class of promising fluorescent probes in biology, chemistry and materials science fields.² In particular, semiconducting polymer dots (Pdots) have attracted considerable attention in the biological field due to their outstanding advantages of simple preparation, small size, high brightness, excellent photostability, and low cytotoxicity.^{3–8} The versatile surface modification also made Pdots expand their applications easily and greatly in various biological fields. Therefore, a number of Pdots have been successfully applied in biosensing, cell imaging, photoacoustic imaging, cancer therapy, *etc.*

Recently, chlorinated organic materials have drawn increased attention due to their interesting properties and they have been applied in many organic electronics fields. As the second-highest electronegative element (Pauling electronegativity for Cl: 3.1614) in the halogen group, the chlorine (Cl) atom shows high capability to hold electron density, which will affect the molecular energy levels (tuning the HOMO and LUMO levels) and absorption

spectra of the resulting organic materials.⁹ The “heavy-atom effect” of the large Cl atom is also able to tune the charge-transporting abilities and emissive characteristics of the resulting materials.¹⁰ Moreover, the chlorinated molecules are easy to access with low cost and chlorine chemistry is more developed when compared with fluorine one, which is very favorable for their practical applications. Despite these distinguishing properties, limited studies concerning Cl-containing semiconductors have been reported, presumably due to the steric hindrance effects originating from the large atomic size of chlorine which may cause harmful effects to its final properties.

It has been proved that the chlorinated molecules showed similar functions to the fluorinated ones in terms of electron transport and device stabilities, according to some reported results (*i.e.*, the chlorinated PDI and NDI derivatives).^{11–15} Stephen R. Forrest *et al.*¹⁶ developed a NIR-absorbing non-fullerene acceptor with a smaller energy gap (1.3 eV) by introducing four Cl atoms, and proved that the chlorination would enhance the intramolecular charge transfer. Hou and co-workers¹⁷ also proved that chlorination was more effective in enhancing the intramolecular charge transfer effect, therefore, the Cl substituted compounds showed more red-shifted absorption spectra when compared with their fluorinated counterparts. Our group also developed a series of chlorinated polymers, which displayed deeper HOMO levels and increased open circuit voltage of their devices, and finally the best power conversion efficiency of 9.11% was achieved.¹⁸ All these results indicate that the chlorinated materials have great potential in various organic electronics, these interesting researches may bring the boom prosperity of chlorinated organic materials in the near future.

^a Institute of Chinese Medical Sciences, University of Macau, 999078, Macao, P. R. China. E-mail: qwzhang@umac.mo

^b Department of Chemistry, Southern University of Science and Technology, Shenzhen, 518055, P. R. China. E-mail: hef@sustc.edu.cn

^c Department of Materials Science and Engineering, South University of Science and Technology, Shenzhen, 518055, P. R. China. E-mail: tianll@sustc.edu.cn

† Electronic supplementary information (ESI) available. See DOI: 10.1039/c8nj05671d

On the other hand, Yang's previous studies proved that the introduction of halogen atoms into phosphorescent molecules could easily tune their emissive lifetimes and photoluminescence quantum yields (QYs).¹⁹ Afterwards, they further proved that the halogenation of the electron acceptor groups in thermally activated delayed fluorescence (TADF) emitters can act as a simple and effective strategy to shorten the delayed lifetimes of TADF emitters while improving their QYs.²⁰ Encouraged by these results, we herein present the chlorination of a benzothiadiazole (BT)-based polymer as a semiconducting polymer to prepare Pdots (**PFDPBCT**). It was found that the Cl atom could increase the QYs and reactive oxygen species (ROS) generation ability of the resulting Pdots when compared with their non-chlorinated counterparts (**PFDPBT** Pdots). The QYs of **PFDPBCT** Pdots dispersed in water could reach 20.3%, while 8.5% was determined for non-chlorinated **PFDPBT** Pdots. Furthermore, in cellular imaging applications, the chlorinated Pdots offered higher brightness than the non-chlorinated Pdots. All these studies showed that these chlorinated Pdots were highly fluorescent and demonstrated their promising potential in bioimaging applications.

Results and discussion

Synthesis and characterization

Fig. 1 shows the synthetic routes of monomers and polymers. All of the monomers were characterized by ¹H NMR spectroscopy and ESI-MS. 2,1,3-Benzothiadiazole,¹⁸ 4,7-dibromo-2,1,3-benzothiadiazole, 5-chloro[2,1,3]benzothiadiazole, 4,7-dibromo-5-chloro-2,1,3-benzothiadiazole,¹⁸ 4,7-diphenyl-2,1,3-benzothiadiazole,²² and 4,7-bis(4-bromophenyl)-2,1,3-benzothiadiazole²² were prepared according to the published procedures. 5-Chloro-4,7-diphenyl-2,1,3-benzothiadiazole was synthesized by a Stille coupling reaction of 5-chloro-2,1,3-benzothiadiazole and tributylstannyl benzene in toluene using Pd₂(dba)₃ and P(*o*-tol)₃ as the catalysts. The bromination of 5-chloro-4,7-diphenyl-2,1,3-benzothiadiazole was conducted under the same conditions as 4,7-diphenyl-2,1,3-benzothiadiazole but the reaction time was increased to 48 h.

The **PFDPBCT** and **PFDPBT** were prepared using the Suzuki polymerization²¹ between monomer 4,7-bis(4-bromophenyl)-2,1,3-benzothiadiazole/4,7-bis(4-bromophenyl)-5-chloro-2,1,3-benzothiadiazole and 2,7-bis(4,4,5,5-tetramethyl-1,3,2-dioxaborolan-2-yl)-9,9-dioctylfluorene with a feed ratio of the monomers of 50:50 and Pd(PPh₃)₄ as the catalyst. The number-average molecular weights (*M_n*) of the **PFDPBCT** and **PFDPBT** were determined to be 12.01 kDa and 9.58 kDa with a polydispersity index (PDI) of 1.5 and 1.6, respectively, characterized by gel permeation chromatography (GPC) with polystyrene as the standard. The smaller *M_n* of the **PFDPBCT** than that of the **PFDPBT** may likely be due to the reduced reactivity of the chlorinated monomers. In the experiments, we found that it was difficult to obtain the bis-substituted products through the Suzuki coupling reaction of 4,7-dibromo-5-chloro-2,1,3-benzothiadiazole and phenylboronic acid. Therefore,

the Stille coupling reaction was used to synthesize the chlorinated monomers. Similarly, the reactivity of chlorinated monomers may be low, and therefore the corresponding *M_n* of **PFDPBCT** was also low. Both polymers showed good solubility in common organic solvents, such as chloroform, toluene, dichloromethane, and tetrahydrofuran, which ensured their solution processing abilities.

The thermal properties of **PFDPBCT** and **PFDPBT** were measured by thermo-gravimetric analysis (Fig. S1, ESI[†]) and differential scanning calorimetry (Fig. S2, ESI[†]), and the results exhibited their good thermal stabilities. The decomposition temperatures (the temperature corresponding to 5% weight loss) of the two polymers were determined to be 347.1 and 352.7 °C, respectively. Finally, a residual weight percentage of about 63% at 600 °C for both the polymers was recorded. In addition, from 50 to 250 °C in the DSC curves, we did not observe an obvious transition change suggesting that all the polymers were amorphous.

The photophysical properties of the **PFDPBT** and **PFDPBCT** were studied by UV-vis spectroscopy and photoluminescence (PL) spectroscopy in dilute THF solutions (Fig. 2a). As shown in Fig. 2a, the bands at *ca.* 340 nm and *ca.* 330 nm in the absorption spectra of **PFDPBT** and **PFDPBCT**, respectively, were attributed to the fluorene segment and the peaks at about 415 nm (**PFDPBT**) and 396 nm (**PFDPBCT**) (Table 1) were attributed to the benzothiadiazole unit incorporated into the polyfluorene main chain.²² It was anticipated that the incorporation of the large chlorine atom could induce a blue-shift of the absorption and fluorescence peaks, as the planarity of the π -backbone and the effective conjugation lengths were decreased by the steric effect of the Cl substituent. This conclusion was also supported by the decreased QYs for the chlorinated polymer (*vide infra*). **PFDPBCT** exhibited a green emission, whose PL peak was at 527 nm, showing a slight blue-shift compared with **PFDPBT** (530 nm). The relatively large Stokes shifts (120 and 131 nm) and high fluorescence QYs (82.6% for **PFDPBT** and 66.9% for **PFDPBCT**) of the polymers are beneficial to increase the resolution for cell imaging.²³ In addition, the relatively lower QYs of the **PFDPBCT** were consistent with the previously reported results due to the structural hindrance of the Cl atom.²⁴

The solvatochromism of fluorescence of **PFDPBT** and **PFDPBCT** was also studied in various solvents of different polarities (Fig. S3 and S4, ESI[†]). The emission spectra of **PFDPBT** and **PFDPBCT** exhibit gradual bathochromic shifts of 51 and 76 nm, respectively, from the local excited (LE) state in poorly polar hexane to the charge-transfer (CT) state in polar *N,N*-dimethylformamide. The higher red-shifts of the CT states in the PL spectra of **PFDPBCT** could be attributed to their different dipole moments in the CT states caused by the stronger electron-withdrawing effect of the Cl groups.²⁵ In addition, the **PFDPBCT** possess partially separated HOMOs and LUMOs, which also could make them easily induce stronger intermolecular charge transfer (Fig. 3), so the solvatochromism of **PFDPBCT** was more obvious.²⁵

The molecular energy levels of **PFDPBT** and **PFDPBCT** were also investigated by cyclic voltammetry (Fig. S5, ESI[†]). Two irreversible

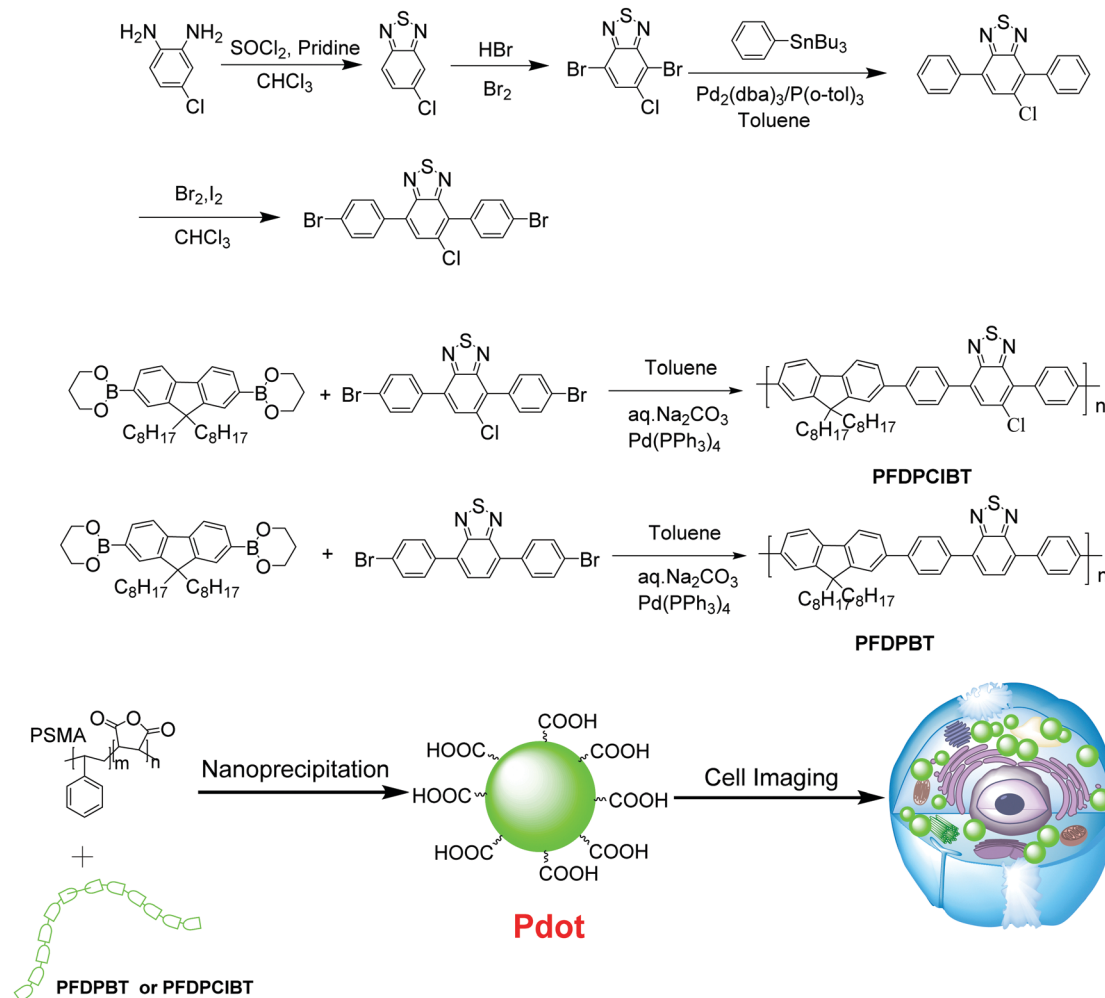


Fig. 1 The synthetic routes for the monomers, polymers, and Pdots.

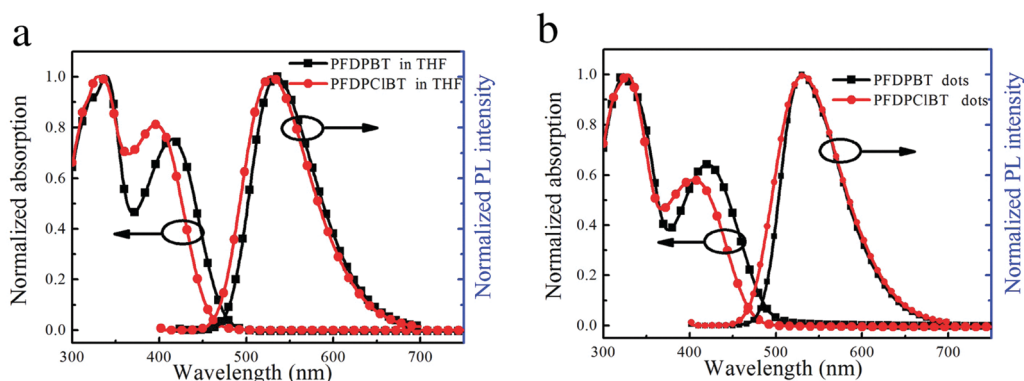


Fig. 2 (a) UV-vis absorption and PL spectra of PFDPBIBT and PFDPBIBT in THF solutions. (b) UV-vis and PL spectra of PFDPBIBT Pdots and PFDPBIBT Pdots in water.

$1e^-$ reduction steps were both observed for the two polymers, and the HOMO energy levels of PFDPBIBT and PFDPBIBT determined from their oxidation onset potentials (E_{ox}) were -6.26 and -6.29 eV ($E_{HOMO} = -(4.80 + E_{ox})$), respectively. It was expected that the HOMO of the PFDPBIBT (-6.29 eV) decreased to a lower level

compared with the H-substituted PFDPBIBT (-6.26 eV) due to the substitution of electron-withdrawing Cl atoms, which was similar to our reported results. To gain deep insights into the electronic properties of the polymers, density functional theory (DFT) calculations were carried out employing Gaussian 09²⁶ software with the

Table 1 Summary of size and photophysical properties of the copolymer in THF solutions and its Pdot form in water

Copolymers	$\lambda_{\text{abs,max(THF)}}^a$ (nm)	$\lambda_{\text{FL,max(THF)}}^b$ (nm)	$\lambda_{\text{abs,max(Pdot)}}^a$ (nm)	$\lambda_{\text{FL,max(Pdot)}}^b$ (nm)	$\Phi(\%)$	Size (nm)
PFDPBT	415	535	422	530	82.6 ^c (8.5 ^d)	72.5 ^e
PFDPICBT	396	527	405	530	66.9 (20.3)	75.2

^a Absorption maximum. ^b Fluorescence maximum. ^c Quantum yield in THF solutions. ^d Quantum yield in Pdot form. ^e Hydrodynamic size measured by DLS.

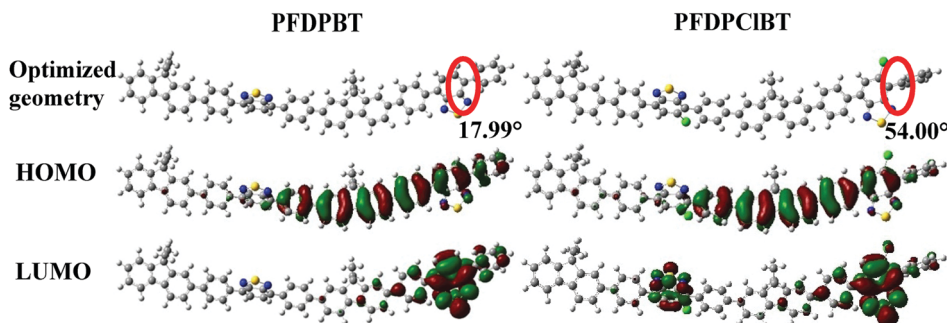


Fig. 3 Minimized energy ground state geometries and the frontier molecular orbital electron density distributions of **PFDPBT** and **PFDPICBT**.

B3LYP functional at the 6-311G(d,p) basis set level. To simplify the calculations, two repeating units of the polymers were used and alkyl groups were replaced by methyl groups. As illustrated in Fig. 3, the dihedral angle between the BT unit and the phenyl unit (near the Cl atom) of **PFDPICBT** was 54.00°, whereas the corresponding angle of **PFDPBT** was 17.99°. The larger dihedral angle of **PFDPICBT** should be attributed to the stronger steric hindrance, which was caused by the introduction of the large Cl atom. The calculated HOMO of **PFDPICBT** (−5.02 eV) was also a little lower than that of **PFDPBT** (−4.90 eV), probably owing to the inductive electron-withdrawing characteristic of the Cl atom. The highest occupied molecular orbital (HOMO) and the lowest unoccupied molecular orbital (LUMO) of **PFDPICBT** were partially separated, which provided the respective channels for the transport of holes and electrons.²⁵ On the other hand, the LUMO position of both **PFDPICBT** and **PFDPBT** was mainly dependent on the acceptor unit (BT-based acceptor group).

Pdots preparation and properties

The two kinds of Pdots were made through rapidly co-precipitating the conjugated polymers of **PFDPBT** (or **PFDPICBT**) and poly(styrene-maleic anhydride) (PSMA). Upon precipitation in deionized water, the polymer backbone folded and distorted due to hydrophobic interactions. As we know, PSMA almost has no influence on the molar absorption coefficient of polymers and has no emission. The hydrophilic maleic anhydride units in PSMA with spontaneous hydrolysis of maleic anhydride groups will be most likely localized on the surface of the Pdots. The TEM images showed that both the Pdots exhibited spherical morphology with an average diameter of 50 nm (Fig. 4a and b). The mean hydrodynamic diameters of **PFDPBT** Pdots and **PFDPICBT** Pdots calculated by dynamic light scattering (DLS) were 72.5 nm and 75.2 nm, respectively (Fig. 4c). The particle size given by TEM was smaller than that by DLS, most likely due to the hydrated Pdots facing shrinkage during TEM sample preparation.²⁷ The zeta-potentials of **PFDPBT** Pdots

and **PFDPICBT** Pdots in aqueous solutions were determined to be −27.3 mV and −18.1 mV, respectively (Fig. 4d). These Pdots are colloiddally stable, with no obvious signs of further aggregation and noticeable leaching from nanoparticle storage for several months.²⁸

Fig. 2b shows the absorption and PL spectra of **PFDPBT** and **PFDPICBT** Pdots. The charge transfer (CT) transition in the long wavelength region for **PFDPBT** Pdots was located at 422 nm, while the CT peak for the **PFDPICBT** Pdots displayed a blue-shift of 17 nm (405 nm) owing to the introduction of chlorine atoms.²¹ As expected, the absorption spectra of both **PFDPBT** Pdots and **PFDPICBT** Pdots in water showed an obvious red-shift compared with those in their THF solutions attributed to the molecular aggregations during the process in forming Pdots. To our surprise, the emission peaks of the **PFDPBT** Pdots and **PFDPICBT** Pdots nearly coincided, which were centered at 530 nm. The absolute QYs for the **PFDPBT** Pdots and **PFDPICBT** Pdots were measured to be 8.5% and 20.3%, respectively. These results indicated that the formed Pdots still retained adequate fluorescence intensities, so they have potential for applications in cell imaging. Table 1 summarizes the photophysical properties of **PFDPBT** Pdots and **PFDPICBT** Pdots, which also clearly indicates that **PFDPICBT** Pdots exhibit higher fluorescence brightness.

The copolymers **PFDPBT** and **PFDPICBT** in THF solutions showed QYs of 82.6% and 66.9%. However, when the two types of Pdots blended with PSMA, the QYs of the Pdots displayed a remarkable difference as discussed above (**PFDPBT** Pdots: 8.5%, **PFDPICBT** Pdots: 20.3%). According to the previously reported results,²¹ we concluded that the hydrophilic group in PSMA played a dominant role in causing the large QY difference between the different types of Pdots. The lower QYs of **PFDPBT** Pdots were likely due to **PFDPBT** chains being aggregated or stacked more densely than when Pdots were formed, leading to great aggregation quenching. In **PFDPICBT** Pdots, the reduced

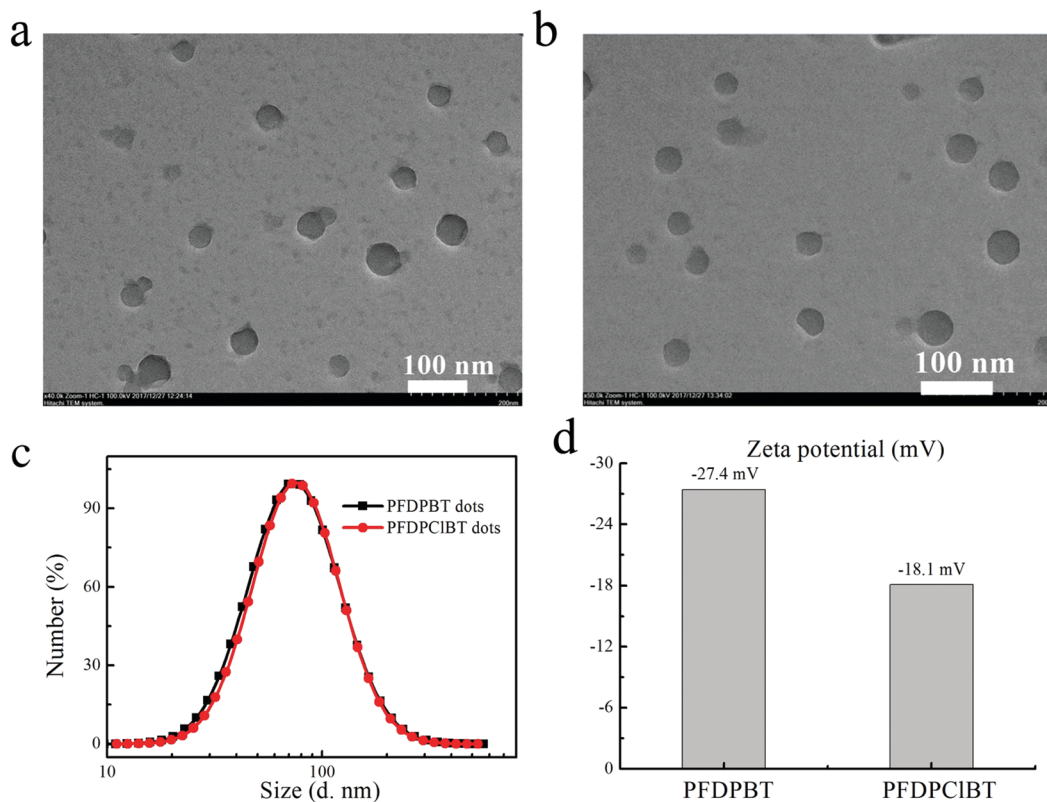


Fig. 4 TEM images of (a) PFDPBt dots and (b) PFDPClBt dots; (c) DLS data and (d) zeta potentials of the PFDPBt dots and PFDPClBt dots.

aggregation-induced quenching tendency was likely due to the following two factors: (1) the intermolecular interactions of Cl-S and Cl-Cl may result in a rigid and extended polymer chain; (2) strong hydrophobic and large structural hindrances of the Cl atoms would make PFDPClBt Pdts stacked loosely when compared with PFDPBt Pdts.²¹

Cell imaging of the Pdts

To further demonstrate the biological applicability of the Pdts for cellular imaging, we first evaluated the cytotoxicity of the two kinds of Pdts by using the MTT method. The results show that these two Pdts exhibited similar biological toxicity. The A549 cells grew normally in the culture medium containing PFDPBt Pdts or PFDPClBt Pdts in the concentration range of 5–80 $\mu\text{g mL}^{-1}$ for 48 h, indicating almost no cytotoxicity of the Pdts (Fig. 5a and b). We next used them to incubate with A549 cells *via* endocytosis for 4 h. The confocal fluorescence microscopy images distinctly revealed that the two kinds of Pdts had got into the cells and accumulated. Both of the Pdts were preferentially stained in the cytoplasm regions of the A549 cells rather than in their nucleic parts. As expected, all the A549 cells stained by the two kinds of Pdts showed high green labeling brightness, which is enough demand for their application in high quality cell imaging. The A549 cells labeled with PFDPClBt Pdts also exhibited much higher emission intensity than the cells labeled with PFDPBt Pdts under identical experimental conditions (Fig. 5c and d). The cellular imaging indicates that the PFDPClBt Pdts are more

suitable for cell imaging, as the higher brightness improves the imaging quality.²⁹

Reactive oxygen species detection

Due to the so-called heavy atom effect, the chlorine group introduced in PFDPClBt Pdts may enhance the singlet oxygen generation (ROS) by spin orbit coupling.³⁰ Herein, to investigate whether PFDPClBt Pdts were able to generate ROS, a 2',7'-dichlorofluorescein diacetate (DCFH) probe was selected as the ROS indicator. As shown in Fig. 6, it was found that the mixed aqueous solutions of DCFH/PFDPClBt Pdts reveal increased PL intensities when exposed to white light irradiation (40 mW cm^{-2}) within 20 minutes (I/I_0 : 1–4.06), while DCFH (I/I_0 : 1–0.94) and DCFH/PFDPBt Pdts (I/I_0 : 1–1.04) show almost negligible fluorescence. All these results demonstrated the stronger singlet oxygen generation ability of PFDPClBt Pdts than PFDPBt Pdts and may find applications in photodynamic therapy in the future.

In addition, a comparison of the ability of generating reactive oxygen species of PFDPClBt Pdts with other photosensitizers has been made. It shows that although the ability of generating reactive oxygen species of PFDPClBt Pdts was higher than that of PFDPBt Pdts, it is still not competitive when compared with the reported values (PFVBT Pdts (I/I_0 : 1–300),³¹ TPE-Py-FFGYSA photosensitizer (I/I_0 : 1–260),³² UCNP/PFVCN nano-hybrids (I/I_0 : 1–400),³³ TPA-BDTP NPs (I/I_0 : 1–80)),³⁴ which show emission in the red/near red region. In general, far-red and near-IR emitting conjugated polymers/

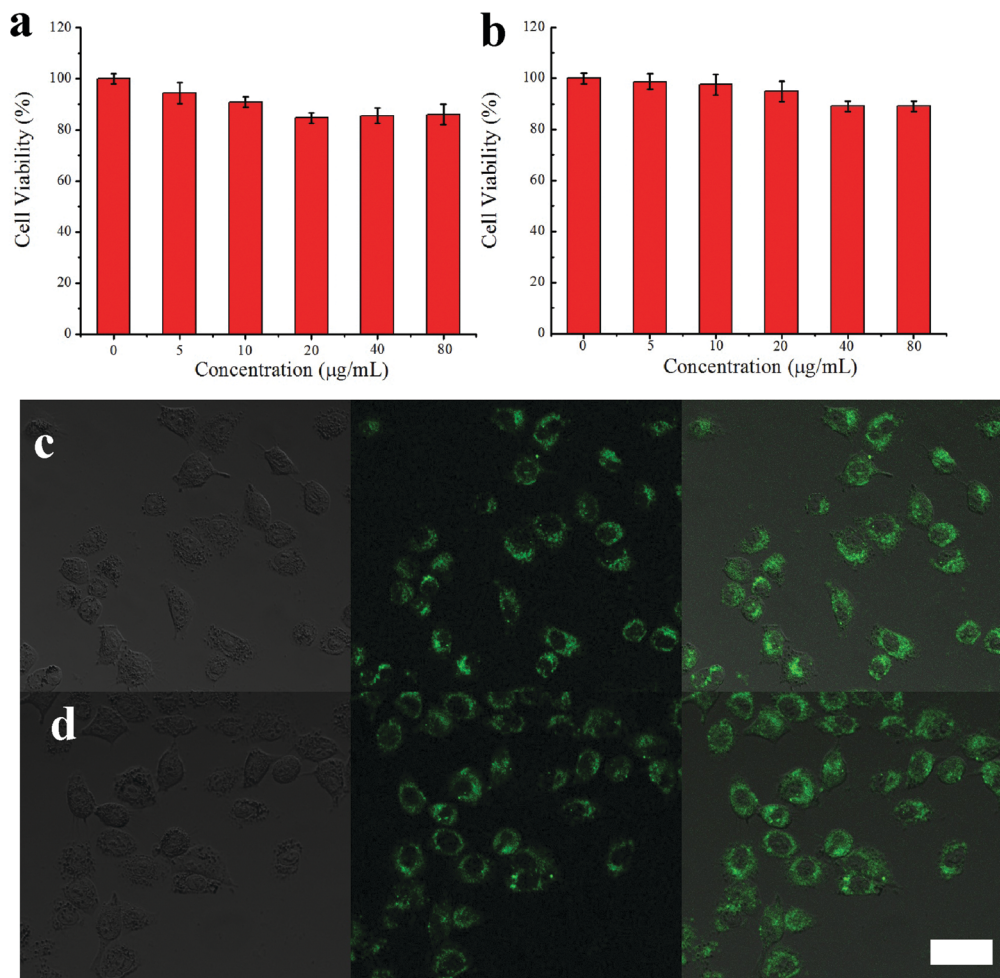


Fig. 5 The cell viability of A549 cells in the culture of different concentrations of (a) **PFDPBT** Pdots and (b) **PFDPICBT** Pdots after incubation for 48 h. Fluorescence imaging of A549 cells incubated with $40 \mu\text{g mL}^{-1}$ (c) **PFDPBT** Pdots and (d) **PFDPICBT** Pdots for 4 h. From left to right are bright field images, fluorescence images, and combined bright field and fluorescence images (scale bar equals $50 \mu\text{m}$).

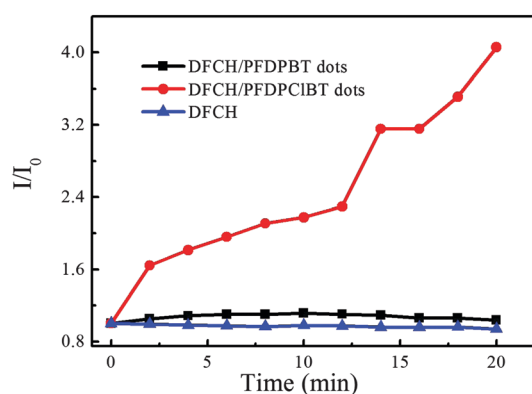


Fig. 6 Plots of I/I_0 (emission intensity)/ I_0 (emission intensity at 0 min) of the DCFH/**PFDPICBT** Pdots, DCFH/**PFDPBT** Pdots, and DCFH versus different light irradiation times.

small molecules can effectively generate ROS and can act as PSs directly without the mediation of any other chromophores.³⁵ Incorporation of photosensitizer (generally porphyrin) into the

PFDPICBT Pdots may significantly improve the production of singlet oxygen generation.³⁶

Photostability of Pdots

To further confirm their potential as effective fluorescent probes, their photostabilities with fluorescein sodium in water were also investigated through 50 min of irradiation with a xenon lamp (100 mW cm^{-2}). We chose fluorescein sodium as control mainly for the following reasons: (1) fluorescein sodium is one of the most stable commercially available fluorescent organic dyes widely used for bioimaging;^{37,38} (2) it has a similar excitation wavelength to **PFDPICBT** Pdots and **PFDPBT** Pdots and very similar emission peaks. As illustrated in Fig. 7, it can be seen that the extent of degradation of UV absorbance of the two Pdots is very small, and the degradation degree of fluorescence is also much lower when compared with fluorescein sodium. At the same time, we can also conclude that chlorinated **PFDPICBT** Pdots show better stability than **PFDPBT** Pdots. The retention of the original absorbance was 92.6% for **PFDPICBT** Pdots after 50 minutes; 82.8% and 6.8% were

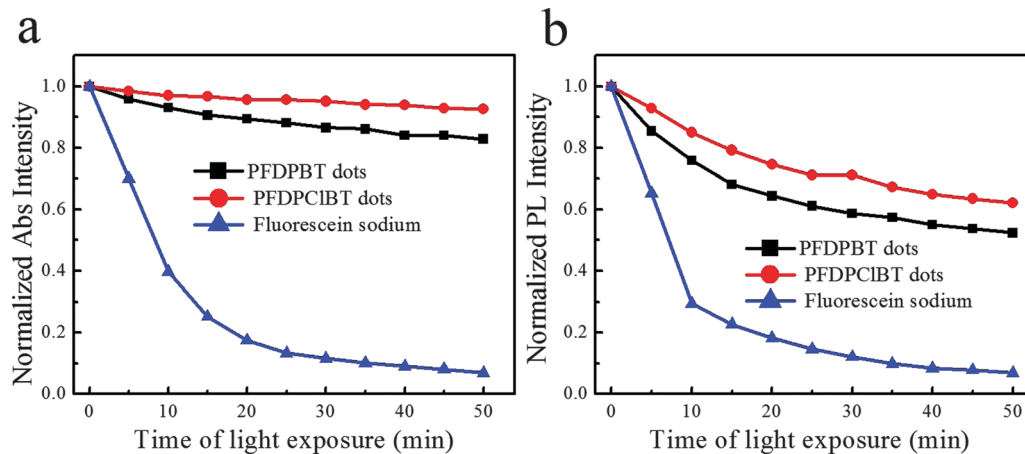


Fig. 7 (a) Time-dependent photodegradation (absorption intensity) and (b) photobleaching (fluorescence intensity) of the PFDPBIBT Pdots and PFDPBT Pdots compared with fluorescein sodium after 50 min of irradiation.

retained for PFDPBT Pdots and fluorescein sodium, respectively (Fig. 7a). On the other hand, the fluorescence intensity of the PFDPBIBT Pdots decreased to 62.1% after 50 min (52.4% for PFDPBT Pdots), and the fluorescein sodium sharply decreased to 6.9% (Fig. 7b). This result was very similar to the results of PFBT Pdots reported by Chiu and co-workers.³⁹ In addition, the Pdots also exhibited greatly improved photostability over many other fluorescent probes such as Au nanoclusters and CdTe QDs.⁴⁰

Conclusions

In summary, we synthesized a novel fluorescent chlorinated semiconducting polymer named PFDPBIBT. The Pdots were prepared by the nanoprecipitation method with an amphiphilic polymer PSMA as the co-encapsulation matrix. TEM measurements indicated that both PFDPBIBT Pdots and PFDPBT Pdots were spherical with an average diameter of about 50 nm. The absorption peak of PFDPBIBT Pdots shows a blue-shift compared with that of non-chlorinated PFDPBT Pdots, which is caused by the incorporation of the large chlorine atom and the steric effect of the Cl substituent that reduces the planarity of the π -backbone. This conclusion is also supported by the decreased QYs of the chlorinated polymer (82.6% for PFDPBT and 66.9% for PFDPBIBT) in THF solutions. However, the PFDPBIBT Pdots have a QY as high as 20.3%, which is much higher than the QY of PFDPBT Pdots (8.5%). The cell imaging study also shows that the brightness of the cells labeled with PFDPBIBT Pdot probes is higher when compared with those labeled with PFDPBT Pdots. The chlorine atom introduced in PFDPBIBT Pdots also enhanced the ability of generating reactive oxygen species and improved the photostability. All these data show that the introduction of the large chlorine atom onto the polymer backbone would result in a significant difference in the photophysical and biological properties of the corresponding Pdots, making them promising probes for biological detection.

Experimental section

Chemicals and reagents

2,7-Bis(4,4,5,5-tetramethyl-1,3,2-dioxaborolan-2-yl)-9,9-dioctylfluorene, 4-chloro-1,2-diaminobenzene, 1,2-diaminobenzene, pyridine, thionyl chloride (SOCl_2), bromine (Br_2), *N*-bromosuccinimide (NBS), iodine (I_2), 2',7'-dichlorofluorescein diacetate (DCFH-DA), tributylstannyl benzene, phenylboric acid, tetrakis(triphenylphosphine)palladium(0) ($\text{Pd}(\text{PPh}_3)_4$), and hydrobromic acid (HBr) were purchased from Energy Chemical (Shanghai, China). Potassium carbonate (K_2CO_3) and sodium carbonate (Na_2CO_3) were obtained from Damao Chemical Reagent Company (Tianjin, China). Tris(dibenzylideneacetone)dipalladium(0) ($\text{Pd}_2(\text{dba})_3$), tri-*o*-tolylphosphine ($\text{P}(o\text{-tol})_3$), and poly(styrene-*co*-maleic anhydride) (PSMA, average $M_w = 1700$, the styrene content was about 68%) were purchased from Sigma-Aldrich. Tetrahydrofuran (THF) and toluene were distilled under nitrogen protection from Na/benzophenone before reaction. Other solvents and reagents were used directly as received. Human alveolar epithelial cells (A549) were kindly provided by Professor Ying Sun at the Department of Biology of Southern University of Science and Technology (SUSTech).

Synthetic procedures

Preparation of 4,7-diphenyl-2,1,3-benzothiadiazole. 4,7-Dibromo-2,1,3-benzothiadiazole (4.93 g, 16.43 mmol), potassium carbonate (27.25 g, 197.2 mmol), $\text{Pd}(\text{PPh}_3)_4$ (0.759 g, 0.6572 mmol), and phenylboric acid (4.24 g, 34.84 mmol) were added into a 250.0 mL round bottom flask. H_2O (69 mL) and toluene (350 mL) were syringed at once. The flask was cooled by liquid nitrogen and blanked by argon three times, then heated at 90 °C for 24 h. After cooling to room temperature, the same volume of water was added to the reaction flask and then extracted with dichloromethane (DCM) several times. The organic layer was washed with saturated aqueous solution of NaCl and dried with anhydrous sodium sulfate (Na_2SO_4). After the solvent was evaporated by rotary distillation under reduced pressure, the title compound (yellow solid) was obtained by column chromatography

(petroleum ether–DCM (5 : 1, v/v)). Yield: 4.62 g (98.3%). ^1H NMR (500 MHz, CDCl_3) δ : 7.99 (d, 4H, J = 8 Hz), 7.82 (s, 2H), 7.59 (t, 4H, J = 8 Hz), 7.52 (d, 2H, J = 8 Hz). ESI-MS: $\text{C}_{18}\text{H}_{12}\text{N}_2\text{S}$ calcd 288.0721, found. 288.0742.

Preparation of 4,7-bis(4-bromophenyl)-2,1,3-benzothiadiazole.

A solution of Br_2 (10 mL, 194 mmol) in chloroform (10 mL) was added slowly into a 250 mL round bottom flask with 30 mL chloroform with dissolved iodine (0.12 g, 0.47 mmol) and 4,7-diphenyl-2,1,3-benzothiadiazole (2.39 g, 8.3 mmol). After stirring at room temperature for 12 h, the reaction mixture was quenched with saturated aqueous Na_2SO_3 solution. The solid was precipitated in water, filtered, and the cake was washed with water and methanol sequentially to give the crude product. Recrystallization from toluene gave the final product as yellow needles. Yield: 2.88 g (78%). ^1H NMR (500 MHz, CDCl_3) δ : 7.87 (d, 4H, J = 8 Hz), 7.80 (s, 2H), 7.70 (d, 4H, J = 8 Hz). ESI-MS: $\text{C}_{19}\text{H}_{14}\text{Br}_2\text{N}_2\text{S}$ calcd 459.9244, found. 459.9267.

Preparation of 5-chloro-4,7-diphenyl-2,1,3-benzothiadiazole.

4,7-Dibromo-5-chloro-2,1,3-benzothiadiazole (2.10 g, 6.40 mmol), tributylstannyl benzene (5.71 g, 15.69 mmol), $\text{Pd}_2(\text{dba})_3$ (290.9 mg), and $\text{P}(o\text{-tol})_3$ (581.8 mg) were added to a 250.0 mL round bottom flask. The flask was blanked by argon three times and 100 mL of toluene was syringed at once and the reaction mixture was stirred at 100 °C for 12 hours. After cooling to room temperature, the organic solvent was removed under reduced pressure. The title compound was obtained by column chromatography (1.89 g, 92.1%) as a light yellow solid. ^1H NMR (500 MHz, CDCl_3) δ : 7.98 (d, 2H, J = 8 Hz), 7.82 (s, 1H), 7.50–7.61 (m, 8H). ESI-MS: $\text{C}_{18}\text{H}_{11}\text{ClN}_2\text{S}$ calcd 322.0311, found. 322.0352.

Preparation of 4,7-bis(4-bromophenyl)-5-chloro-2,1,3-benzothiadiazole. 4,7-Bis(4-bromophenyl)-5-chloro-2,1,3-benzothiadiazole was synthesized in a similar manner to 4,7-bis(4-bromophenyl)-2,1,3-benzothiadiazole, and the reaction time was increased to 48 h. Yield: 1.82 g (78%). ^1H NMR (500 MHz, CDCl_3) δ : 7.87 (m, 3H), 7.79 (d, 2H, J = 8 Hz), 7.50–7.63 (m, 4H). ESI-MS: $\text{C}_{18}\text{H}_9\text{Br}_2\text{ClN}_2\text{S}$ calcd 493.8855, found. 493.8873.

General procedure of Suzuki polymerization

PFDPBT. 2,7-Bis(4,4,5,5-tetramethyl-1,3,2-dioxaborolan-2-yl)-9,9-dioctylfluorene (120 mg, 0.19 mmol), 4,7-bis(4-bromophenyl)-2,1,3-benzothiadiazole (85.15 mg, 0.19 mmol), $\text{Pd}(\text{PPh}_3)_4$ (6 mg, 0.005 mmol), and Bu_4NBr (2.45 mg, 0.0076 mmol) were added into a 25 mL flask. Then, 4 mL of toluene and 2 mL of aqueous Na_2CO_3 (2 M) were added using a syringe. The flask was frozen by liquid nitrogen, degassed, and refilled with argon three times. The mixture was heated to 90 °C with vigorous stirring for two days under an argon atmosphere. After cooling to room temperature, the mixture was re-precipitated into 100 mL methanol, then filtered and washed with methanol, acetone and distilled water in turn. Then, the crude product was dissolved in 15 mL THF, filtered through a 0.22 μm micron filter and re-precipitated in 100 mL methanol. The powder was stirred in acetone for 24 hours, filtered and dried in a vacuum oven (102.7 mg, 79.5%). ^1H NMR (500 MHz, CDCl_3) δ : 8.15 (br, 4H), 7.92 (br, 9.52H), 7.71 (br, 5.31H), 7.73 (br, 1.35H), 2.10 (br, 4.48H), 1.14 (br, 24.67H), 0.84 (br, 12.53 H). M_n (GPC): 12.01 k, D : 2.03.

PFDPICBT. PFDPICBT was prepared by a similar method used to prepare PFDPBT using monomers 4,7-dibromo-5-chloro-2,1,3-benzothiadiazole and 2,7-bis(4,4,5,5-tetramethyl-1,3,2-dioxaborolan-2-yl)-9,9-dioctylfluorene. Yield: 84.9%. ^1H NMR (500 MHz, CDCl_3) δ : 8.14 (br, 2.81H), 7.99 (br, 1H), 7.93 (br, 6.83H), 7.72 (br, 6.58H), 7.61 (br, 3.40H), 2.12 (br, 4.94H), 1.14 (br, 26.16 H), 0.84 (br, 13.08 H). M_n (GPC): 9.58 k, D : 1.33.

Measurements

^1H and ^{13}C NMR spectra were obtained using a Bruker Avance-500 (500 MHz) spectrometer. The molecular weight and molecular weight distribution of the synthesized polymers were measured with gel permeation chromatography (GPC) at 40 °C on a Malvern Viscotek 270 max system equipped with a UV detector, using polystyrene (Aldrich) as the standard and THF as the eluent. The UV-vis spectra were obtained using a Shimadzu UV-3600 PC by using 1 cm quartz cuvettes. The fluorescence spectra of the polymers in THF solution and Pdots in aqueous solution were obtained using a Shimadzu RF5301 PC fluorescence spectrometer. The absolute QYs were measured using an integrating sphere system, and were determined on a Horiba Jobin Yvon-Edison Fluoromax-4 fluorescence spectrometer. Time-dependent photodegradation and photobleaching experiments were carried out using a xenon lamp (100 mW cm^{-2}). The fluorescence of DCF was excited at 488 nm and collected within 500–545 nm. Particle sizes were measured using a Hitachi H-600 transmission electron microscope (TEM) and a NanoBrook Omni dynamic light scattering instrument (DLS, Brookhaven Instruments Corporation). For the TEM measurements, the Pdot solution (about 20 μL) was placed on a carbon-coated copper grid. After evaporation of the water at room temperature, morphology of the Pdots was measured using a Hitachi H-600 instrument.

Preparation of Pdots

PFDPBT and PFDPICBT were firstly dissolved in THF at a concentration of 1000 $\mu\text{g mL}^{-1}$, respectively. At the same time, the same concentration of PSMA (1000 $\mu\text{g mL}^{-1}$) in THF was also prepared. 500 μL PFDPBT solution or PFDPICBT solution, 100 μL PSMA, and 9400 μL THF were mixed together to form a homogeneous solution. Under ultrasound conditions, 5 mL of the mixed solution was quickly injected into 10 mL of deionized water. The excess THF was removed by heating under nitrogen stripping and the solution was concentrated to about 5 mL. After that, a 0.22 micron filter was used to filter the solution to remove the fraction of aggregates. The size and morphology of the Pdots were characterized by TEM and DLS and stored in a refrigerator (4 °C) until further use.⁴¹

Cytotoxicity studies

The cytotoxicities of PFDPBT Pdots and PFDPICBT Pdots were measured by MTT assay. First, A549 cells were seeded in 96-well plates at a number of 5×10^3 cells per well and incubated for 24 h and 48 h (37 °C, 5% CO_2). The cells were then grown in the medium at a series of concentrations of Pdots (0, 5, 10, 20, 40, and 80 $\mu\text{g mL}^{-1}$). After 24 hours, 20 μL of MTT (5 mg mL^{-1} in PBS) was added, the culture medium was removed carefully,

and then 150 μL DMSO was added to dissolve the formazan after shaking gently for 10 minutes. The absorbance at the 490 nm wavelength was recorded using a microplate reader (Cytation3, Biotek, USA).

Cell imaging

For the cell uptake, the cultured A549 cells (1.5×10^4) were digested and plated onto glass-bottomed microscope dishes and allowed to grow for 12 h. Then, the dispersions of **PFDPBT** dots ($\sim 40 \mu\text{g mL}^{-1}$) and **PFDPICBT** dots ($\sim 40 \mu\text{g mL}^{-1}$) were separately added to the cell culture solution and further cultured for 4 hours. Finally, the glass-bottomed dishes were washed at room temperature with $1 \times$ PBS (pH 7.4) buffer and placed on the fluorescence microscope for cell imaging.

Conflicts of interest

There are no conflicts to declare.

Acknowledgements

This work was financially supported by the National Natural Science Foundation of China (51773087, 21733005, 51503096, 51603100), the Natural Science Foundation of Guangdong Province (2016A030313637), Shenzhen Fundamental Research program (JCYJ20160504151536406, JCYJ20160504151731734), Shenzhen Nobel Prize Scientists Laboratory Project (C17783101), the Research Committee of the University of Macau (MYRG2016-00046-ICMS-QRCM), Guangzhou Science and Technology, and the Guangzhou International Science and Technology Collaboration Funding from the Guangzhou Science Technology and Innovation Commission (R&D of cephalotaxine-type compounds as new anti-chronic myeloid leukemia drugs, EF010/ICMS-ZQW/2018/GSTIC).

Notes and references

- L. Feng, C. Zhu, H. Yuan, L. Liu, F. Lv and S. Wang, *Chem. Soc. Rev.*, 2013, **42**, 6620–6633.
- C. Zhu, L. Liu, Q. Yang, F. Lv and S. Wang, *Chem. Rev.*, 2012, **112**, 4687–4735.
- J. Pecher and S. Mecking, *Chem. Rev.*, 2010, **110**, 6260–6279.
- D. Tuncel and H. V. Demir, *Nanoscale*, 2010, **2**, 484–494.
- K. Li and B. Liu, *J. Mater. Chem.*, 2012, **22**, 1257–1264.
- A. Kaeser and A. P. H. J. Schenning, *Adv. Mater.*, 2010, **22**, 2985–2997.
- K. Pu and B. Liu, *Adv. Funct. Mater.*, 2011, **21**, 3408–3423.
- K. Li and B. Liu, *Chem. Soc. Rev.*, 2014, **43**, 6570–6597.
- H. Wang, P. Chao, H. Chen, Z. Mu, W. Chen and F. He, *ACS Energy Lett.*, 2017, **2**, 1971–1977.
- F. Yang, C. Li, W. Lai, A. Zhang, H. Huang and W. Li, *Mater. Chem. Front.*, 2017, **1**, 1389–1395.
- M. Tang, J. Oh, A. Reichardt and Z. Bao, *J. Am. Chem. Soc.*, 2009, **131**, 3733–3740.
- M. Gsnger, J. H. Oh, M. Knemann, H. W. Hffken, A. M. Krause, Z. Bao and F. A. Wrthner, *Angew. Chem., Int. Ed.*, 2010, **49**, 740–743.
- J. H. Oh, S. L. Suraru, W. Y. Lee, M. Konemann, H. W. Hoffken, C. Roger, R. Schmidt, Y. Y. Chung, W. Chen, F. Wurthner and Z. Bao, *Adv. Funct. Mater.*, 2010, **20**, 2148–2156.
- T. He, M. Stolte and F. Würthner, *Adv. Mater.*, 2013, **25**, 6951–6955.
- M. Nakano, I. Osaka, D. Hashizume and K. Takimiya, *Chem. Mater.*, 2015, **27**, 6418–6425.
- Y. Li, J. Lin, X. Che, Y. Qu, F. Liu, L. Liao and S. R. Forrest, *J. Am. Chem. Soc.*, 2017, **139**, 17114–17119.
- Y. Cui, C. Yang, H. Yao, J. Zhu, Y. Wang, G. Jia, F. Gao and J. Hou, *Adv. Mater.*, 2017, **29**, 1703080.
- D. Mo, H. Wang, H. Chen, S. Qu, P. Chao, Z. Yang, L. Tian, Y. Su, Y. Gao, B. Yang, W. Chen and F. He, *Chem. Mater.*, 2017, **29**, 2819–2830.
- C. Fan, L. Zhu, B. Jiang, Y. Li, F. Zhao, D. Ma, J. Qin and C. Yang, *J. Phys. Chem. C*, 2013, **117**, 19134–19141.
- Y. Xiang, Y. Zhao, N. Xu, S. Gong, F. Ni, K. Wu, J. Luo, G. Xie, Z. Lu and C. Yang, *J. Mater. Chem. C*, 2017, **5**, 12204–12210.
- Y. Zhang, J. Yu, M. E. Gallina, W. Sun, Y. Rong and D. T. Chiu, *Chem. Commun.*, 2013, **49**, 8256–8258.
- J. Liu, L. Bu, J. Dong, Q. Zhou, Y. Geng, D. Ma, L. Wang, X. Jing and F. Wang, *J. Mater. Chem.*, 2007, **17**, 2832–2838.
- C. Yan, Z. Sun, H. Guo, C. Wu and Y. Chen, *Mater. Chem. Front.*, 2017, **1**, 2638–2642.
- D. Mo, S. Zhen, J. Xu, W. Zhou, B. Lu, G. Zhang, Z. Wang, S. Zhang and Z. Feng, *Synth. Met.*, 2014, **198**, 19–30.
- L. Han, K. Ye, C. Li, Y. Zhang, H. Zhang and Y. Wang, *ChemPlusChem*, 2017, **82**, 315–322.
- T. Korzdorfer and J. L. Bredas, *Acc. Chem. Res.*, 2014, **47**, 3284–3291.
- Y. Fan, J. Zhao, Q. Yan, P. Chen and D. Zhao, *ACS Appl. Mater. Interfaces*, 2014, **6**, 3122–3131.
- H. Chen, J. Zhang, K. Chang, X. Men, X. Fang, L. Zhou, D. Li, D. Gao, S. Yin, X. Zhang, Z. Yuan and C. Wu, *Biomaterials*, 2017, **144**, 42–52.
- X. Fang, Y. Zhang, K. Chang, Z. Liu, X. Su, H. Chen, S. Zhang, Y. Liu and C. F. Wu, *Chem. Mater.*, 2016, **28**, 6628–6636.
- J. Yang, X. Gu, W. Su, X. Hao, Y. Shi, L. Zhao, D. Zou, G. Yang, Q. Li and J. Zou, *Mater. Chem. Front.*, 2018, **2**, 1842–1846.
- G. Feng, Y. Fang, J. Liu, J. Geng, D. Ding and B. Liu, *Small*, 2017, **13**, 1602807–1602818.
- C. Chen, Z. Song, X. Zheng, Z. He, B. Liu, X. Huang, D. Kong, D. Ding and B. Tang, *Chem. Sci.*, 2017, **8**, 2191–2198.
- J. Li, Q. Zhao, F. Shi, C. Liu and Y. Tang, *Adv. Healthcare Mater.*, 2016, **5**, 2967–2971.
- S. Zhen, S. Wang, S. Li, W. Luo, M. Gao, L. Ng, C. Goh, A. Qin, Z. Zhao, B. Liu and B. Tang, *Adv. Funct. Mater.*, 2018, **28**, 1706945–1706959.
- T. Senthilkumar and S. Wang, *Conjugated Polymers for Biological and Biomedical Applications*, Wiley, Hoboken, NJ, USA, 2018.

- 36 S. Li, K. Chang, K. Sun, Y. Tang, N. Cui, Y. Wang, W. Qin, H. Xu and C. Wu, *ACS Appl. Mater. Interfaces*, 2016, **8**, 3624–3634.
- 37 M. Lan, J. Zhang, X. Zhu, P. Wang, X. Chen, C. S. Lee and W. Zhang, *Nano Res.*, 2015, **8**, 2380–2389.
- 38 J. Zhang, R. Chen, Z. Zhu, C. Adachi, X. Zhang and C. S. Lee, *ACS Appl. Mater. Interfaces*, 2015, **7**, 26266–26274.
- 39 C. Wu, T. Schneider, M. Zeigler, J. Yu, P. G. Schiro, D. R. Burnham, J. D. McNeill and D. T. Chiu, *J. Am. Chem. Soc.*, 2010, **132**, 15410–15417.
- 40 C. Chen, P. Wu, S. Liou and Y. Chan, *RSC Adv.*, 2013, **3**, 17507–17514.
- 41 F. Ye, C. Wu, Y. Jin, M. Wang, Y. Chan, J. Yu, W. Sun, S. Hayden and D. T. Chiu, *Chem. Commun.*, 2012, **48**, 1778–1780.